Synthesis of sol-gel pyrophyllite/TiO_2 heterostructures: Effect of calcination temperature and methanol washing on photocatalytic activity

Abdelali El Gaidoumi[a,b,*], José Miguel Doña Rodríguez[a], Elisenda Pulido Melián[a], Oscar Manuel González-Díaz[a], José Antonio Navío Santos[c], Brahim El Bali[b], Abdelhak Kherbeche[b]

[a] Grupo de Fotocatálisis y Espectroscopia Aplicada al Medioambiente (FEAM, Unidad Asociada al CSIC por el Instituto de Ciencias de Materiales de Sevilla),Centro Instrumental Químico-Físico para el Desarrollo de Investigación Aplicada (CIDIA)-Dpto. de Química, Edificio Central del Parque Científico Tecnológico, Universidad de Las Palmas de Gran Canaria, Campus Universitario de Tafira, 35017 Las Palmas, Spain

[b] Laboratoire de Catalyse, Matériaux et Environnement (LCME), Ecole Supérieure de Technologie de Fès, Université Sidi Mohamed Ben Abdellah, 30000 Fès, Morocco

[c] Instituto de Ciencia de Materiales de Sevilla, Centro Mixto CSIC-Universidad de Sevilla and Dpto. de Química Inorgánica, Universidad de Sevilla, Avda.Américo Vespucio s/n, 41092 Sevilla, Spain

* Corresponding author. Abdelali El Gaidoumi. Tel.: +212652206015.
E-Mail: elgaidoumi.abdelali@hotmail.fr (A. El Gaidoumi).

ABSTRACT

We successfully synthesized an efficient photoactive pyrophyllite/TiO_2 heterostructures using a sol-gel route at ambient temperature. The samples were prepared by exfoliation of a pyrophyllite layered-type clay by TiO_2. The prepared samples exhibited strong photocatalytic activity for the degradation of phenol. The heterostructure PTi750 (S_{BET} = 16.58 m^2/g) calcined at 750°C, in which the mixed phases of anatase and rutile exist (52.2% anatase/10.7% rutile), showed the highest photocatalytic activity against commercial TiO_2 Aeroxide P25. The methanol washed PTi750 was 5 times faster than the corresponding unwashed sample; phenol was totally degraded with a TOC reduction of 89.2%. The materials have been characterized by: X-ray diffraction (XRD), Diffuse reflectance UV-vis spectrophotometry (UV-Vis DRS), scanning electron microscopy (SEM) and BET specific surface area.

Keywords: Sol-gel; Pyrophyllite; Heterostructure; Photocatalysis; Methanol washing

1. Introduction

The water pollution becomes a serious environmental problem in over the world because of quick industrialization and urbanization which prompt a continuous release of toxic pollutants from industrial, agricultural and sewage waste into the encompassed water bodies which oftentimes cause water pollution. The majority of the water polluted by industrial effluents containing toxic pollutants is discharged in natural water bodies without appropriate treatment. The advanced oxidation processes (AOPs) are conventional methods for the removal of toxic pollutants from aqueous solutions. AOPs are concern all the processes based on generation of strong oxidation radicals (usually, hydroxyl radicals) able to degrade and eliminate contaminants of waters [1, 2]. Among them are ozonation, sonolysis, Fenton oxidation and photocatalysis as well as combinations. Photocatalysis is one of AOPs that has attracted great attention of researchers in the last years. It is extensively used for decomposition of organic contaminants and gases in waters and air [3, 4]. In this sense, our research group has reported the photodegradation of some toxic organics substances in liquid medium, such as phenolic compounds [5], acids [6], herbicides [7] and fungicides [8], and NO_x in gas medium [9]. Titanium dioxide (TiO_2) is a typical photocatalyst utilized for environmental treatment, mainly because of its UV light-responsive properties, ability to catalyze the oxidation of toxic organic pollutants to nontoxic products, such as CO_2 and H_2O, low cost, chemical inertness, photostability, non-toxicity, non-corrosion and recyclability [10, 11].

Using porous materials for assembling or immobilizing nanostructured semiconductors may be an alternative to design porous photocatalysts with higher adsorption properties, while maintaining electronic and structural properties appropriate for application in water treatment. The process consists in fixing semiconductors onto several supports, like zeolites [12], activated carbon [13] or clay minerals [14, 15]. Various layered clay-based materials have been used in photocatalysis such as acid-modified clays, modified organoclays, semiconductor-clay heterojunctions, pillared clays (PILCs) [16-18] or the so-called Porous Clay Heterostructures (PCHs), described by a higher porous properties [19] and Delaminated Porous Clay Heterostructures (DPCHs), described by the exfoliation of the clay layers producing more developed porous materials [20-24].

Pyrophyllite, a relatively rare mineral, is a layered hydroxy-aluminosilicate with dioctahedral 2:1 structure (Fig. 1). Its crystal structure is described in terms of Al-O(OH) octahedral sheets sandwiched between two tetrahedral SiO_4 sheets, with each octahedral Al

bonded with the tetrahedral Si by an apical O and with an adjacent Al by two OH groups [25]. Pyrophyllite exhibits good physico-chemical characteristics such as low electrical and thermal conductivity, low expansion coefficient, low thermal expansion, low reversible and excellent reheating stability [26]. It has been widely used in many industries, particularly in ceramics, rubbers paints fiber glasses, plastic, paper, fire-brick, cosmetic manufacture of refractories insulating materials and porous materials. Most of these applications are due to its good technological properties following thermal treatment [26]. Moreover, several researches have been performed on the use of pyrophyllite as an adsorbent of some contaminants as like cyanide [27], boron ions [28] and heavy metals [29-31]. In this paper, we report on the pyrophyllite/TiO_2 heterostructures, which belong to DPCHs materials. They have been synthesized by a sol-gel route hydrolyzing the titanium tetrabutoxide (IV) precursor with the pyrophyllite layered-type clay, at ambient temperature, followed by the calcination at different temperatures. The activity of resulting photocatalysts was tested in the photodegradation of phenol under UV irradiation and it proved promising results, compared to the commercial TiO_2 Aeroxide P25.

2. Experimental

2.1. Products

The natural clay used in this work comes from the south of Morocco, mainly pyrophyllite, was already investigated by our group [32-36]. Its composition (wt%) is: SiO_2 (57.9%), Al_2O_3 (25.5%), Fe_2O_3 (2.71%), K_2O (1.6%), Na_2O (1.53%), MgO (0.83%), TiO_2 (0.64%) and CaO (0.12%). It was used in this work after decarbonation with 0.5 M hydrochloric acid under stirring [32]. Aeroxide P25, which was used as reference photocatalyst, phenol (≥99.5%), titanium (IV) t-butoxide (97%), hydrochloric acid (37%), acetonitrile (≥99.8 %) and methanol (99.8%) were supplied by Sigma-Aldrich; ethanol (≥99.5 %) was supplied by Panreac. All reagents were directly used without further purification. All solutions were prepared using dionized water prepared from a Milli-Q Millipore system.

2.2. Synthesis of the photocatalysts

The synthesis of the pyrophyllite/TiO_2 heterostructures followed a sol-gel technique that consists on reacting layered pyrophyllite clay with TiO_2, which comes from the titanium tetrabutoxide hydrolysis. Firstly, adding dropwise a solution made of 8.5 mL of titanium (IV) tetrabutoxide (TiTB) and 20 mL of ethanol to a solution consisting in 10 mL of ethanol in

which 1 g of decarbonated clay (PT), sieved with a 63 µm mesh, is dispersed, under magnetic agitation. After continuous agitation (15 min), a solution of 15 mL of ethanol diluted with 10 mL of distilled water was added drop by drop until a spontaneous gelation, giving then place to a dense gel, which was leaved to age for 24 h. After a washing series with water, this gel was dried at 100 °C for 24 h, this will be symbolized there below "TiTB-PT". The dried solid was sieved with a 63 µm mesh and then calcined at various temperatures between 450 and 850 °C for 4 h. The prepared heterostructures are symbolized "PTiX" where X represents calcination temperature. The methanol washed PTi750 (hereinafter noted Wsh-PTi750), which methanol washing has been done before calcination step, was also tested.

2.3. Characterizations techniques

X-ray diffraction (XRD) analyzes were performed using a Siemens D-500 difractometer ($\lambda_{CuK\alpha}$ = 1.5418 Å) in the range of 10°-80°. Phase crystalline sizes in the different samples were estimated from the line broadening of the corresponding XRD peaks by using the Debye-Scherrer (Eq. 1) [37]:

$$D = \frac{K\lambda}{\beta \, Cos(\square)} \quad (1)$$

where D is the average crystallite size (nm), λ the X-ray wavelength of Cu K_α radiation (λ = 0.15432 nm), K the shape factor (K = 0.89), β the full-width at half maximum (FWHM) intensity of the (101) plane and □ is the Bragg angle.

The relative percentage to anatase and rutile in TiO_2 proportion was estimated using Spurr-Myers (Eq. 2) [38] as follows:

$$A(\%) = 100 - R(\%) = \frac{100 \, I_A}{I_A + 1.265 \, I_R} \quad (2)$$

where A (%) and R (%) are the relative percentages to anatase and rutile, respectively, I_A and I_R are the intensities of the anatase (101) peak at 2□ = 25.3° and the rutile (101) peak at 2□ = 27.2°.

Diffuse reflectance UV-vis spectroscopy measurements (UV-vis DRS) were recorded in the region 250-800 nm with a Varian Cary 5 UV-NIR spectrometer. Surface morphology of the photocatalysts was measured by scanning electron microscopy (SEM) using a Jeol JSM-5400 microscope. BET specific surface area was measured by a Micromeritics ASAP 2420

accelerated surface area and porosimetry system, with liquid nitrogen cooling bath (-195.78 °C).

2.4. Oxidation experiments and analytical techniques

The photocatalysis experiments were carried out in 500 mL cylindrical reactor of Pyrex. Aqueous suspensions containing 200 mL of 50 mg. L^{-1} phenol and 1 g.L^{-1} photocatalyst amount were stirred and air-bubbled continuously (400 mL.min^{-1}). UV illumination was carried out outside of reactor. The withdrawn samples were filtered using a filter Millipore (0.45 µm) before being HPLC-analyzed.

The residual phenol concentrations at different reaction times were HPLC-measured using a Supelco Discovery C18 (25 cm×4.6 mm ID, 5 µm particles) column, an acetonitrile-water (30:70) as mobile phase and a UV detector (λ = 270 nm). Total organic carbon (TOC) was measured with a TOC-V_{SCN} analyzer (Shimadzu).

3. Results and discussion

3.1. Characterization studies

3.1.1. Crystallographic and surface area

Fig. 2 shows the XRD patterns of the clay PT, PTiX photocatalysts calcined at temperatures ranging from 450 °C to 850 °C, and Wsh-PTi750. The PT sample exhibits typical peaks of the pyrophyllite ($Al_2(Si_4O_{10})(OH)_2$) and supplementary ones assigned to quartz as impurity, as reported in the literature [39-41]. From PTiX photocatalysts XRD patterns, the transformation of the TiTB precursor to the TiO_2 phase starts at all selected calcination temperatures. The anatase TiO_2 appears in all photocatalysts at 2□ = 25.3°, 37.9°, 48.1°, 53.9°, 55.1°, 62.7° and 63.2°, 68.8° [42-45] while the rutile TiO_2 appears only in samples PTi750 and PTi850 at 2□ = 27.4°, 36.1°, 54.3° and 56.6° [46]. The results show that the washing with methanol has no effect on crystalline phases of PTi750. The peaks ascribed to the pyrophyllite material were observed in XRD patterns of all photocatalysts, which implied that pyrophyllite retained its phase in their structures.

Table 1 shows the surface areas and distribution of anatase and rutile phases in terms of weight composition and particle size of synthesized photocatalysts. All heterostructures show a high value of surface area in comparison with the starting clay, due to the exfoliation of clay layers caused by TiO_2 nanoparticles which favors the accessibility to the internal surface of

the layers [47]. It can also be seen that the calcination temperature increases with increase of particle size of both anatase and rutile and decrease of surface area [5]. The synthesis of the heterostructures implies the creation of mesopores as an important issue confirmed by a significant contribution of mesoporosity according to the values of the external (non-microporous) surface area (Table 1). These mesopores are mainly distributed within a pore diameter range of 3-4 nm (Fig. 3a). The porous structure of the heterostructures, as a result of the presence of clay layers [47], was also confirmed based on the corresponding nitrogen adsorption-desorption isotherms (Fig. 3b). All samples show a type II isotherm (IUPAC classification) with a H3 hysteresis loop [48, 49], except PTi450 which shows a combination of both types I and II [49]. These kinds of isotherms have been described for several layered materials, characterized by porous aggregates due to the "house of cards" structure formed by the plate-like particles [50, 51].

3.1.2. UV-vis DRS characterization

Diffuse reflectance spectra (Fig. 4) of photocatalysts have been carried out, from which band-gap values have been determined (Table 1). From the obtained band gaps, all photocatalysts absorb in the UV region, at a wavelength varying between 385 nm and 398 nm. Remarquably, the PTiX band gaps decrease when rising of calcination temperature. Rising the calcination temperature increased the size of the particles and improved their crystallinity (Table 1). As a result, the defects are reduced and consequently the e-/h+ recombination is reduced. On the other hand, when the crystalline particles are very small, the well-known "quantum size effect" is produced, which leads to an increase in the band gap [52]. This effect has also been mentioned in other studies, in which increased band gap was correlated with decreased particle size caused by faster e-/h+ recombination [5, 53, 54].

3.1.3. SEM characterization

To ensure that the TiO_2 particles are well dispersed on the clay´s surface, a SEM analysis was performed of PT and PTiX heterostructures (Fig. 5). SEM image of PT illustrates that it possesses a layered structure (Fig. 5a), while those of the PTiX heterostructures (Fig. 5b-f) show that TiO_2 particles are assembled and incorporated to the clay layers.

3.2. Photodegradation of phenol

3.2.1. Photoactivity of PTiX heterostructures

Before testing the photocatalysts, an adsorption preliminary test was carried out for 1 h without irradiation (Fig. 6). The results show that the time needed to reach equilibrium varies between 25 min and 30 min. Aeroxide P25 has a low adsorption percentage (0.9%) and PTi650 has the highest adsorption percentage (16.3%) which can be explained by the proportion of contained clay (37.3%). In addition, blank experiments showed that the degradation of phenol was low in the absence of photocatalysts or UV light irradiation. The adsorption phenomenon was eliminated after 30 min for all photocatalysts and then UV light irradiation was started, indicating the start of photocatalytic degradation reaction (t = 0).

Fig.7 shows the evolution of phenol degradation and mineralization in terms of photocatalyst type. In the case of heterostructures, it is found that their photoactivity increases with the calcination temperature, up to 850 °C at which it begins to decrease. PTi750 is the most active among the studied photocatalysts, with degradation and mineralization rates (%) of 91 and 80, respectively.

Figs. 8a and 8b depict the plot of $Ln(C/C_o)$ vs. irradiation time and reaction apparent first order rate constants k_{app} estimated for photocatalytic degradation of phenol with the different photocatalysts, respectively. The results show that PTi750 has the best reactivity justified by the higher value of kapp (0.019 min^{-1}); 1.38 times faster than that of Aeroxide P25 (kapp = 0.014 min^{-1}).

3.2.2. Methanol washing effect

Before using Wsh-PTi750, it was tested in adsorption for 1 h. This photocatalyst shows 17 % of removal at equilibrium time of 20 min (Fig. 9a). Just after this period, UV irradiation was activated, Fig. 9b. illustrates the obtained results. The phenol was totally degraded with 89.2% of TOC reduction after 2 h of irradiation. The plot of Ln (C/C_0) vs. time revealed an apparent first order rate constant of 0.097 min^{-1}. This value, 5 times higher than that obtained without methanol washing, implies the positive effect of this step. The specific surface area of Wsh-PTi750 is 56.39 $m^2.g^{-1}$, it is big larger compared to 16.58 $m^2.g^{-1}$ from the unwashed PTi750 (Table 1). Park et al. studied the ethanol washing effect on textural properties of the sodium silicate-derived silica xerogel and got similar results [55]. Increasing PTi750's surface area caused by methanol washing improved its photoactivity. In fact that increasing in surface area means the creation of a greater number of adsorption sites which are beneficial to the photoactivity [5]. Furthermore, the difference of mechanical properties between PTi750 and Wsh-PTi750 also affected the photoactivity. Once dispersed in the liquid, the methanol molecules had to diffuse in order to access the anatase and rutile crystals contained in

photocatalyst particles. Consequently, the larger pore size of Wsh-PTi750 (Fig. 3a), promotes the diffusion of methanol molecules as well.

The porous structure of Wsh-PTi750 is affected by the surface tension of the methanol. During drying procedure, as the liquid evaporated, the gas/liquid surface within pores was curved and then presented a surface tension which withdrawn the porous wall closer. The higher surface tension results in larger decrease in pore size. The decreasing of pore size favored by the surface tension of water was more significant than that of methanol during the drying step might be explained by the fact that the surface tension of water is greater than that of methanol at room temperature. Therefore, the Wsh-PTi750 had a larger specific surface area and pore size, and showed high activity.

3.2.3. Stability of PTi750 and Wsh-PTi750

After photocatalytic test, the photocatalysts PTi750 and Wsh-PTi750 have been reused after filtration, water washing and drying. Fig. 10 illustrates the results obtained after five cycles of reuse. It is noted that the activity is not significantly lost; the degradation efficiency is about 88.7% for PTi750 and 97.8% for Wsh-PTi750 after five cycles of reuse. This result indicates that these photocatalysts were stable and allowed for possible reuse.

4. Conclusions

Novel pyrophyllite/TiO_2 heterostructures were successfully synthesized, at ambient temperature, via a sol-gel method. The layer structure of decarbonated pyrophyllite was destroyed to some extent and a new dual mesoporous structure was formed by embedding the TiO_2 particles in the clay layers. The heterostructure PTi750 with mixed phases of anatase and rutile showed the higher photocatalytic activity under UV light than that of the commercial Aeroxide P25 in photodegradation of phenol. Meanwhile, the methanol washed PTi750, which is successfully prepared by methanol washing before calcination, showed excellent photocatalytic activity for the degradation of phenol. 2 h of UV photocatalytic reaction with 1 $g.L^{-1}$ amount of this photocatalyst is favorable for total degradation of 200 mL of phenol at 50 $mg.L^{-1}$ concentration and its mineralization over 89 %. The results suggested that PTi750 heterostructure is promising for water purification applications for its good photocatalytic properties.

Acknowledgments

We thank the Ministry of Economy and Competitiveness of the Government of Spain, for its financial support through the infrastructure project 2010-3E UNLP10-3E-726. The LCME laboratory of Sidi Mohamed Ben Abdellah University of Fez, Morocco, gratefully acknowledge collaborations of FEAM group, University of Las Palmas, Spain, during the mobility of Dr. Abdelali El Gaidoumi under Erasmus Plus Key Action 107 Program.

References

[1] O. Gimeno, M. Carbajo, F.J. Beltrán, F.J. Rivas, Phenol and substituted phenols AOPs remediation, J. Hazard. Mater. 119 (2005) 99-108.

[2] S. Vilhunen, M. Sillanpä, Recent developments in photochemical and chemical AOPs in water treatment: a mini-review, Rev. Environ. Sci. Biotech. 9 (2010) 323-330.

[3] G. Marci, A. Sclafani, V. Augugliaro, L. Palmisano, M. Schiavello, Influence of some aromatic and aliphatic compounds on the rate of photodegradation of phenol in aqueous suspensions of TiO_2, J. Photochem. Photobiol. A: Chem. 89 (1995) 67-74.

[4] K. Kočí, V. Matějka, P. Kovář, Z. Lacný, L. Obalová, Comparison of the pure TiO_2 and kaolinite/TiO_2 composite as catalyst for CO_2 photocatalytic reduction, Catal. Today 161 (2011) 105-9.

[5] J. Araña, J.M. Doña-Rodríguez, D. Portillo-Carrizo, C. Fernández- Rodríguez, J. Pérez-Peña, O. González Díaz, J.A. Navío, M. Macias, Photocatalytic degradation of phenolic compounds with new TiO_2 catalysts, Appl. Catal. B: Environ. 100 (2010) 346-354.

[6] E.I. Seck, J. M. Doña Rodríguez, C. Fernández-Rodríguez, O.M. González-Díaz, J. Araña, J. Pérez-Peña, Photocatalytic removal of 2,4-dichlorophenoxyacetic acid by using sol-gel synthesized nanocrystalline and commercial TiO_2: Operational parameters optimization and toxicity studies, Appl. Catal. B: Environ. 125 (2012) 28-34.

[7] O.M. González Sánchez, J. Araña, O. González Díaz, J.A. Herrera Melián,J.M. Doña Rodríguez, J. Pérez Peña, Detoxification of the herbicide propanil by means of Fenton processand TiO_2-photocatalysis, J. Photochem. Photobiol. A Chem. 291 (2014) 34-43.

[8] Dunia E. Santiago, M.R. Espino-Estévez, Gabriel V. González, J. Araña,O. González-Díaz, J.M. Doña-Rodríguez, Photocatalytic treatment of water containing imazalil using animmobilized TiO_2 photoreactor, Appl. Catal. A: General 498 (2015) 1-9.

[9] M.J. Hernández Rodríguez, E. Pulido Melián, O. González Díaz, J. Araña, M. Macías, A. González Orive, J.M. Doña Rodríguez, Comparison of supported TiO2 catalysts in the photocatalytic degradation of NO_x, J. Mol. Catal. A: Chem. 413 (2016) 56-66.

[10] A. Di Paola, E. García-López, G. Marcì, L. Palmisano, A survey of photocatalytic materials for environmental remediation, J. Hazard. Mater. 211-212 (2012) 3-29.

[11] M. Anpo, M. Takeuchi, The design and development of highly reactive titanium oxide photocatalysts operating under visible light irradiation, J. Catal. 216 (2003) 505-516.

[12] A. Corma, H. Garcia, Zeolite-based photocatalysts, Chem. Commun. 13 (2004) 1443-1459.

[13] J.-M. Herrmann, J. Matos, J. Disdier, C. Guillard, J. Laine, S. Malato, J. Blanco, Solar photocatalytic degradation of 4-chlorophenol using the synergistic effect between titania and activated carbon in aqueous suspension, Catal. Today 54 (1999) 255–265.

[14] J. Liu, G. Zhang, Recent advances in synthesis and applications of clay-based photocatalysts: a review, Phys. Chem. Chem. Phys. 16 (2014) 8178-8192.

[15] K. Sahel, M. Bouhent, F. Belkhadem, C. Guillard, F. Figueras, Photocatalytic degradation of anionic and cationic dyes over TiO_2 P25, and Ti-pillared clays and Ag-doped Ti-pillared clays, Appl. Clay Sci. 95 (2014) 205-210.

[16] S. Yang, G. Liang, A. Gu, H. Mao, Synthesis of TiO_2 pillared montmorillonite with ordered interlayer mesoporous structure and high photocatalyticactivity by an intra-gallery templating method , Mater. Res. Bull. 48 (2013) 3948-3954.

[17] D. Papoulis, S. Komarneni, A. Nikolopoulou, P. Tsolis-Katagas, D. Panagiotaras, G.H. Kacandes, P. Zhang, S. Yin, T. Sato, H. Katsuki, Palygorskite- and Halloysite-TiO_2 nanocomposites: Synthesis and photocatalytic active, Appl. Clay Sci. 50 (2010)118-124.

[18] S. Perathoner, G. Centi, Catalytic wastewater treatment using pillared clays, in: A. Gil, S.A. Korili, R. Trujillano, M.A. Vicente (Eds.) , Pillared Clays and Related Catalysts, Springer, New York. 2010, pp. 167-200.

[19] L. Chmielarz, B. Gil, P. Kustrowski, Z. Piwowarska, B. Dudek, M. Michalik, Montmorillonite-based porous clay heterostructures (PCHs) intercalated withsilica-titania pillars: synthesis and characterization , J. Solid State Chem. 182 (2009) 1094-1104.

[20] C. Belver, J. Bedia, J.J. Rodriguez, Zr-doped TiO_2 supported on delaminated clay materials for solarphotocatalytic treatment of emerging pollutants , J. Hazard. Mater. 322 (2017) 233-242.

[21] C. Belver, J. Bedia, M.A. Álvarez-Montero, J.J. Rodriguez, Solar photocatalytic purification of water with Ce-doped TiO_2/clayheterostructures, Catal. Today 266 (2016) 36-45.

[22] C. Belver, J. Bedia, J.J. Rodriguez, Titania-clay heterostructures with solar photocatalytic applications, 176 (2015) 278-287.

[23] P. Aranda, C. Belver, E. Ruiz-Hitzky, Inorganic heterostructured materials based on clay minerals, in: L.F. Drummy, M. Ogawa, P. Aranda (Eds.), Clays and MaterialsCMS Workshop Lectures Series 18, The Clay Minerals Society, Chantilly (VA), 2013, pp. 21-40.

[24] C. Belver, P. Aranda, M.A. Martín-Luengo, E. Ruiz-Hitzky, New silica/alumina-clay heterostructures: Properties as acid catalysts, Microp. Mesop. Mater. 147 (2012) 157-166.

[25] S. Mohammadnejad, J.L. Provis, J.S.J. van Deventer, Effects of grinding on the preg-robbing behaviour of pyrophyllite, Hydrometallurgy 146 (2014) 154-163.

[26] J. Zhang, J. Yan, J. Sheng, Dry grinding effect on pyrophyllite-quartz natural mixture and its influence on the structural alternation of pyrophyllite, Micron 71 (2015) 1-6.

[27] S. Saxena, M. Prasad, S.S. Amritphale, N. Chandra, Adsorption of cyanide from aqueous solutions at pyrophyllite surface, Sep. Purif. Technol. 24 (2001) 263-270.

[28] R. Keren, D.L. Sparks, Effect of pH and Ionic Strength on Boron Adsorption by Pyrophyllite, Soil. Sci. Soc. Am. J. 58 (1994) 1095-1100.

[29] R.G. Ford, D.L. Sparks, The Nature of Zn Precipitates Formed in the Presence of Pyrophyllite, Environ. Sci. Technol. 34 (2000) 2479-2483.

[30] M. Prasad, S. Saxena, S.S. Amritphale, N. Chandra, Kinetics and Isotherms for Aqueous Lead Adsorption by Natural Minerals, Ind. Eng. Chem. Res. 39 (2000) 3034-3037.

[31] A.M. Scheidegger, G.M. Lamble, D.L. Sparks, Investigation of Ni Sorption on Pyrophyllite: An XAFS Study, Environ. Sci. Technol. 30 (1996)548-554.

[32] A. El Gaidoumi, A. Loqman, A. Chaouni Benadallah, B. El Bali, A. Kherbeche, Co(II)-pyrophyllite as Catalyst for Phenol Oxidative Degradation: Optimization Study Using Response Surface Methodology, Waste Biomass Valor. (2017). https://doi.org/10.1007/s12649-017-0117-5.

[33] A. El Gaidoumi, A. Chaouni Benabdallah, B. El Bali, A. Kherbeche, Synthesis and Characterization of Zeolite HS Using Natural Pyrophyllite as New Clay Source, Arab. J. Sci. Eng. 43 (2018) 191-197.

[34] A. El Gaidoumi, J.M. Doña-Rodríguez, E. Pulido Melián, O.M. González-Díaz, B. El Bali, J.A. Navío, A. Kherbeche, Mesoporous pyrophyllite-titania nanocomposites: synthesis and activity in phenol photocatalytic degradation, Res. Chem. Interm. (2018). https://doi.org/10.1007/s11164-018-3605-8.

[35] A. El Gaidoumi, A. Chaouni Benabdallah, A. Lahrichi, A. Kherbeche, Adsorption du phénol en milieu aqueux par une pyrophyllite Marocaine brute et traitée (Adsorption of

phenol in aqueous medium by a raw and treated Moroccan pyrophyllite), J. Mater. Environ. Sci. 6 (2015) 2247-2259.

[36] A. El Gaidoumi, J.M. Doña-Rodríguez, E. Pulido Melián, O.M. González-Díaz, J.A. Navío, B. El Bali, A. Kherbeche, Catalytic efficiency of Cu-supported pyrophyllite in heterogeneous catalytic oxidation of phenol, Arab. J. Sci. Eng. (2018).

[37] A.L. Patterson, The Scherrer formula for X-ray particle size determination, Phys. Rev. 56 (1939) 978-983.

[38] R.A. Spurr, H. Myers, Quantitative analysis of anatase rutile mixtures with an X-ray diffractometer, Anal. Chem. 29 (1957) 760-762.

[39] A. Bentayeb, M. Amouric, J. Olives, A. Dekayir, A. Nadiri, XRD and HRTEM characterization of pyrophyllite from Morocco and its possible applications , Appl. Clay Sci. 22 (2003) 211- 221.

[40] G. Li, J. Zeng, J. Luo, M. Liu, T. Jiang, G. Qiu, Thermal transformation of pyrophyllite and alkali dissolution behavior of silicon, Appl. Clay Sci. 99 (2014) 282-288.

[41] M. Erdemoğlu, S. Erdemoğlu, F. Sayılkan, M. Akarsu, Ş. Şener, H. Sayılkan, Appl. Clay Sci. 27 (2004) 41-52.

[42] N. Hamzah, N.M. Nordinc, A.H.A. Nadzri, Y.A.Nik, M.B. Kassim, M.A. Yarmo, Enhanced activity of Ru/TiO_2 catalyst using bisupport, bentonite-TiO_2 for hydrogenolysis of glycerol in aqueous media, Appl. Catal. A: General 419- 420 (2012) 133-141.

[43] X. Zhao, J. Li, Y. Zhang, H. Dong, J. Qu, T. Qi, Preparation of nanosized anatase TiO_2-coated illite composite pigments by $Ti(SO_4)_2$ hydrolysis, Powder Technology 271 (2015) 262-269.

[44] X. Zhao, J. Li, Y. Liu, Y. Zhang, J. Qu, T. Qi, Preparation and mechanism of TiO_2-coated illite composite pigments, Dyes and Pigments 108 (2014) 84-92

[45] L. Gao, X. Zhan,Y. Lu, J. Li, Q. Sun, pH-dependent structure and wettability of TiO_2-based wood surface, Mater. Lett. 142(2015) 217-220.

[46] J. Li, Suyoulema, W. Wang, Sarina, A study of photodegradation of sulforhodamine B on Au–TiO2/bentonite under UV and visible light irradiation, Solid State Sci. 11 (2009) 2037-2043.

[47] C. Belver, J. Bedia, J.J. Rodriguez, Titania–clay heterostructures with solar photocatalytic applications, Appl. Catal. B: Environ. 176-177 (2015) 278-287.

[48] K.S.W. Sing, R.T.Williams, The use of molecular probes for the characterization of nanoporous adsorbents, Particle Particle Syst. Charact. 21 (2004) 71-79.

[49] J. Rouquerol, F. Rouquerol, P. Llewellyn, G. Maurin, K.S.W. Sing, Adsorption by powders and porous solids: Principles Methodology and Applications, Academic Press, Oxford, 2013.

[50] H. Bel Hadjltaief, M.E. Galvez, M. Ben Zina, P. Da Costa, TiO_2/clay as a heterogeneous catalyst in photocatalytic/photochemical oxidation of anionic reactive blue 19, Arab. J. Chem. (2014). 10.1016/j.arabjc.2014.11.006

[51] A. Gil, S. A. Korili, M. A. Vicente, Recent Advances in the Control and Characterization of the Porous Structure of Pillared Clay Catalysts, Catal. Rev 50(2008) 153-221.

[52] H. Lin, C.P. Huang, W. Li, C. Ni, S. Ismat Shah, Yao-Hsuan Tseng, Size dependency of nanocrystalline TiO_2 on its optical property and photocatalytic reactivity exemplified by 2-chlorophenol, Appl. Catal. B Environ. 68 (2006) 1–11.

[53] S. Liu, N. Jaffrezic, C. Guillard, Size effects in liquid-phase photo-oxidation of phenol using nanometer-sized TiO_2 catalysts, Appl. Surf. Sci. 255 (2008) 2704-2709.

[54] P. Calza, E. Pelizzetti, K. Mogyorosi, R. Kun, I. Dekany, Size dependent photocatalytic activity of hydrothermally crystallized titania nanoparticles on poorly adsorbing phenol in absence and presence of fluoride ion, Appl. Catal. B: Environ. 72 (2007) 314-321.

[55] M. Park, V.C. Menton, S. Komarneni, Ethanol washing effect on textural properties of the sodium sioicate-derived silica xerogel, J. Sol-Gel Sci. Technol. 12 (1998) 15-20.

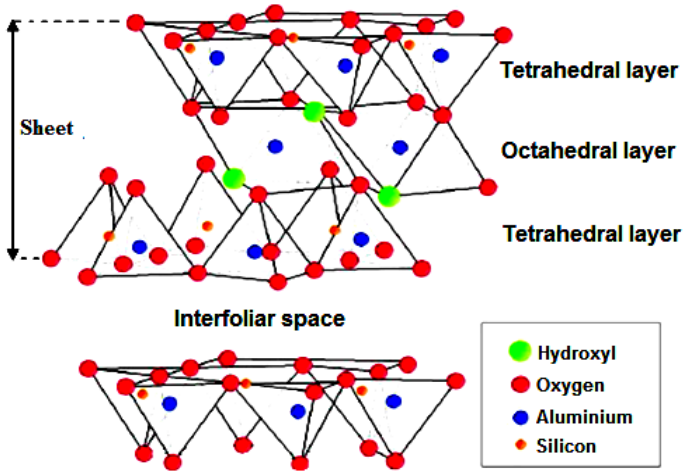

Fig. 1. Structure of pyrophyllite.

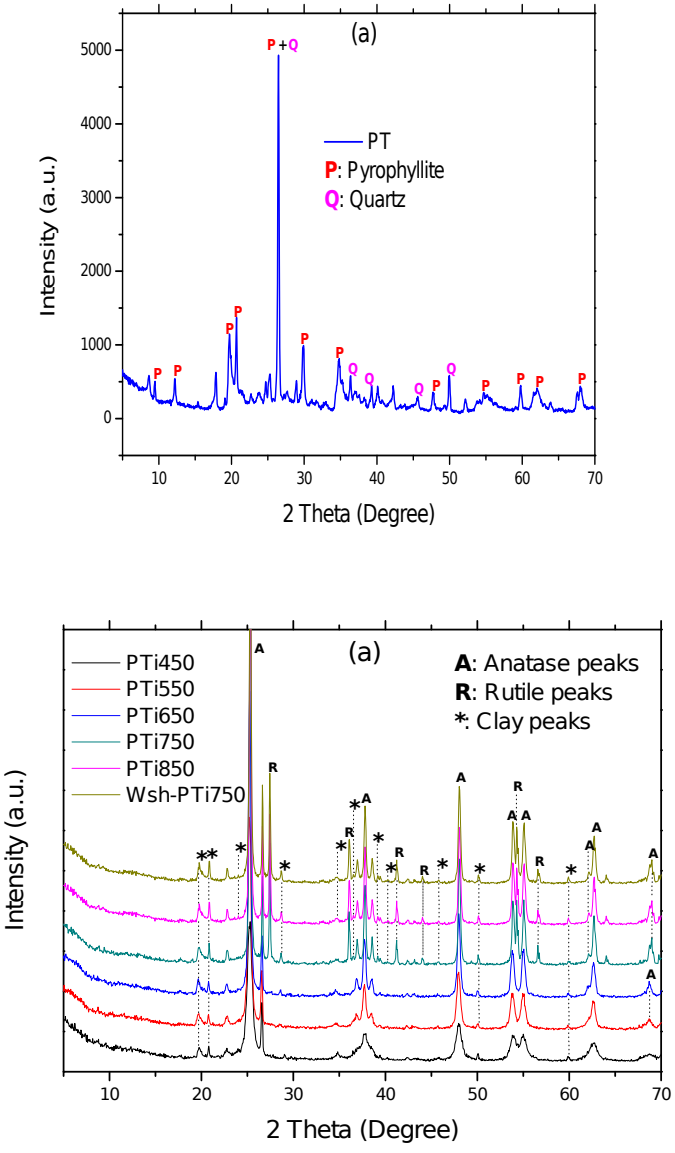

Fig. 2. XRD pattern of (a) PT and (b) photocatalysts.

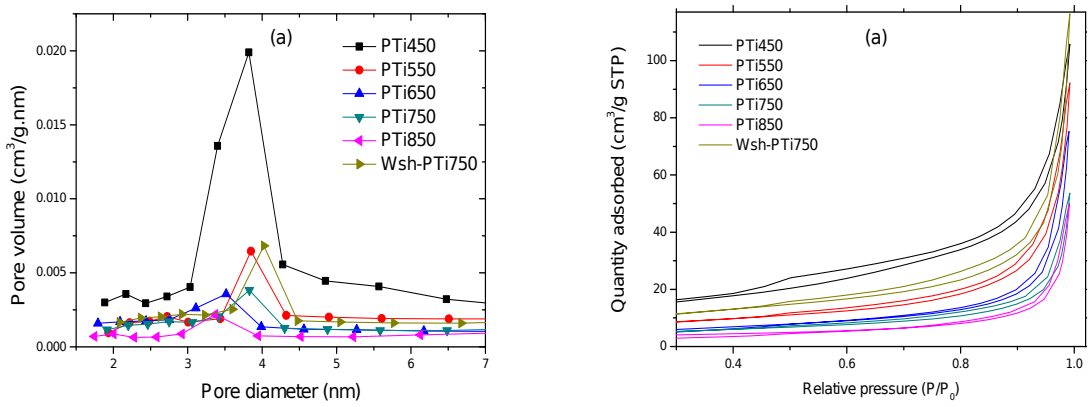

Fig. 3. (a) Pore size distribution and (b) N_2 adsorption-desorption isotherms of photocatalysts.

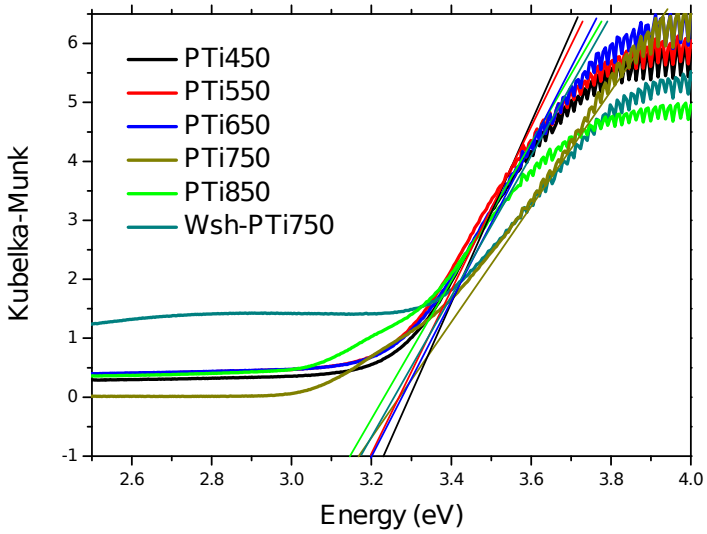

Fig. 4. UV-Vis DRS spectra of different photocatalysts.

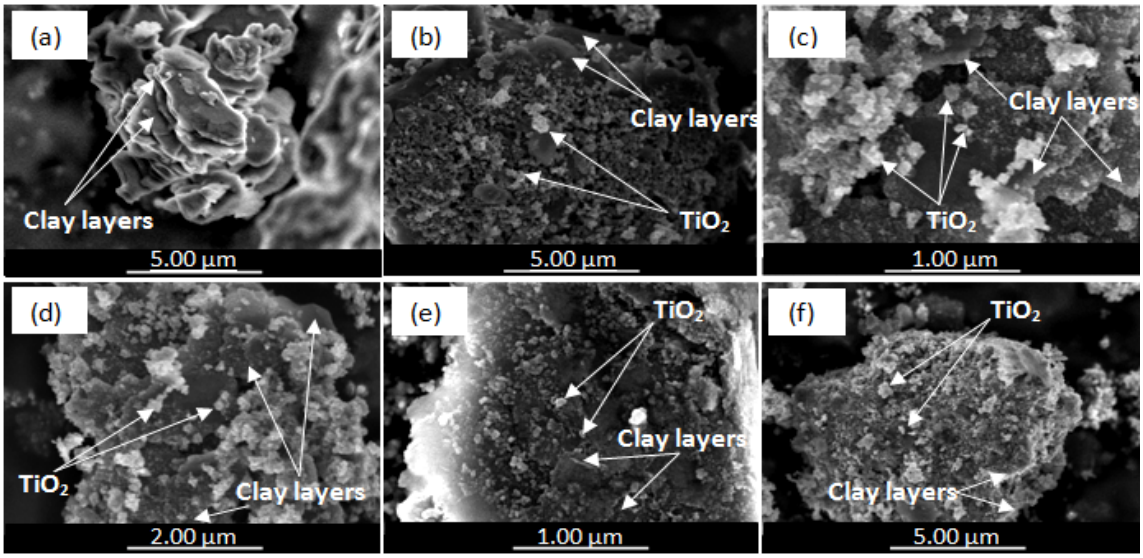

Fig. 5. SEM images: (a) PT, (b) PTi450, (c) PTi550, (d) PTi650, (e) PTi750, (f) PTi850.

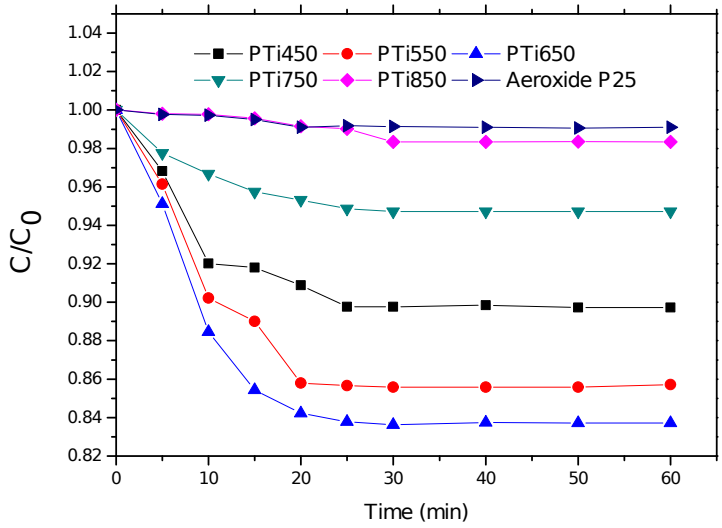

Fig. 6. Evolution of adsorption rate of phenol by PTiX and Aeroxide P25 photocatalysts.

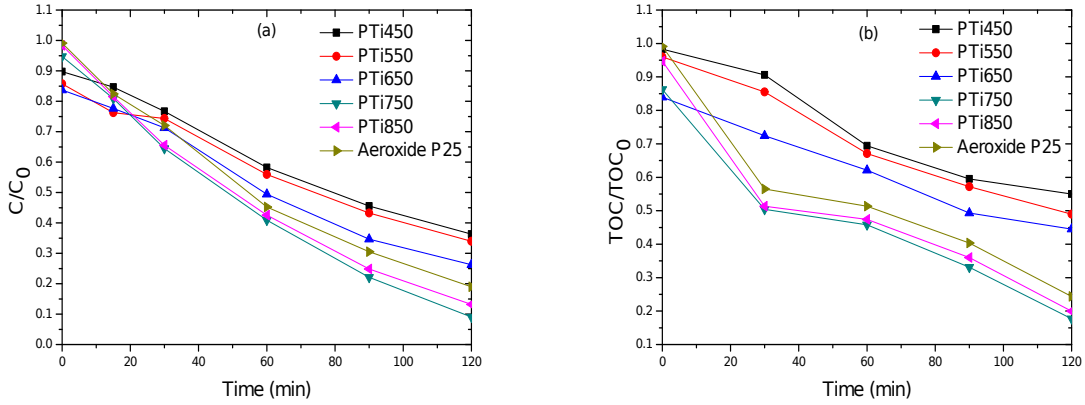

Fig. 7. Evolution of (a) degradation and (b) TOC reduction of phenol rates with PTiX and Aeroxide P25 photocatalysts.

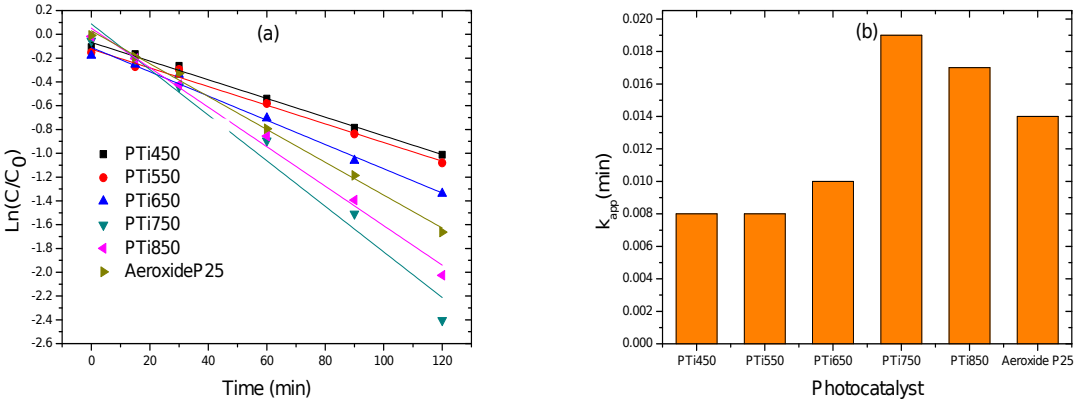

Fig. 8. (a) Plots of Ln(C/C_0) versus time of photocatalysts; (b) Apparent photodegradation rate constants for 50 $mg.L^{-1}$ of phenol with PTiX and Aeroxide P25 photocatalysts.

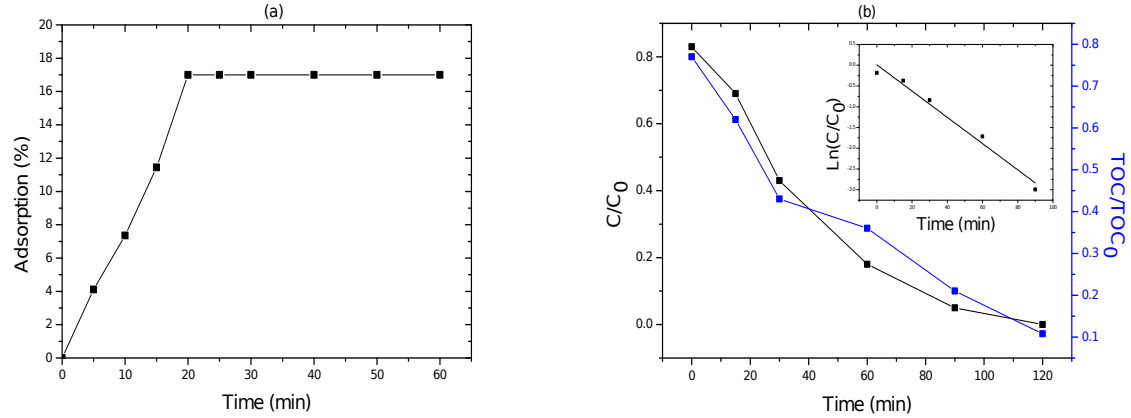

Fig. 9. (a) Evolution of adsorption efficiency and (b) degradation and TOC reduction rates of phenol with Wsh-PTi750.

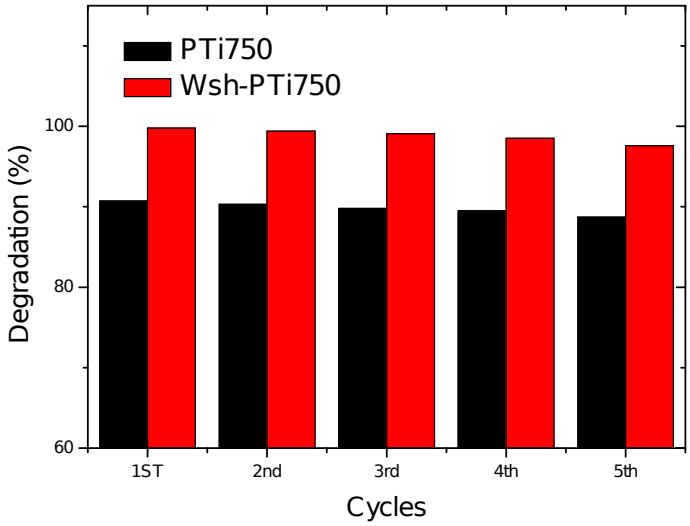

Fig. 10. Reuse cycles of PTi750 and w-PTi750.

Table 1

Percentage of anatase-rutile phases, crystalline size, surface area and band-gap of the different photocatalysts.

Samples	Anatase (A)/Rutile (R) ratio	Cristalline size (nm)		Surface area (m^2/g)		Band gap (eV)
		Anatase	Rutile	S_{BET}	S_{EXT}	
PT	-	-	-	9.14	7.35	-
TiTB-PT	-	-	-	82.21	80.36	-
P25	80% A/20% R	22.1	24.8	52	51.22	3.19
PTi450	61.8% A/0% R	13.7	-	49.12	48	3.23
PTi550	62.2% A/0% R	19.1	-	27.08	24.54	3.21
PTi650	62.7% A/0% R	25.5	-	18.45	17.27	3.21
PTi750	52.2% A/10.7% R	35.5	60.8	16.58	15,74	3.17
PTi850	51.8% A/10.9% R	35.8	62.8	12.74	11.85	3.15
Wsh-PTi750	52.3% A/10.5% R	35.1	60.5	56.39	55,96	3.17